Synaptic Noise-Like Activity in Hippocampal Interneurons

by

David Arthur Stanley

A thesis submitted in conformity with the requirements
for the degree of Masters of Applied Science

Graduate Department of Electrical and Computer Engineering
University of Toronto

Synaptic Noise-Like Activity in Hippocampal Interneurons

David A. Stanley

Masters of Applied Science

Electrical and Computer Engineering
University of Toronto

2009

Abstract

Noise-like activity (NLA) refers to spontaneous subthreshold fluctuations in membrane potential. In this thesis, we examine the role that synaptic channel fluctuations play in contributing to NLA by comparing a detailed biophysical model to experimental data from whole-intact hippocampal interneurons. To represent the contribution from synaptic channel fluctuations, we switch the synapses in the model from traditional to Markovian formalisms and demonstrate statistically relevant increases the standard deviation; power-law scaling exponent; and power spectral density in the 5-100 Hz and 1-5 kHz ranges. However, while synaptic channel fluctuations have a definite effect, we found that they were significantly more subtle than the synaptic response to network activity. This indicates that synaptic channel fluctuations do indeed play a significant role in subthreshold noise, but, overall, synaptic NLA is dominated by the synaptic response to presynaptic network activity.

Acknowledgments

First and foremost, I would like to thank my supervisor, Berj Bardakjian: his guidance and feedback have allowed me to undertake this project, and his continued energy, motivation, and enthusiasm have been instrumental in allowing me to bring it to a successful conclusion. I also wish to acknowledge the support of Dr. Peter Carlen and his PhD student Demitre Serletis, both of whom have provided me with a great deal of advice and inspiration. And, of course, I also wish to acknowledge Demitre for contributing the essential experimental data and helping with the analysis. Finally, I would like to thank my fellow group members, Angela, Demitre, Eunji, Josh, Marija, Sinisa and Osbert for their conversations and advice. Special thanks go to Josh for editing the manuscript and helping me to tame the compiler, Osbert for supplying Matlab code used for despiking traces, and Marija for providing some key insights interpreting the raw data. Special thanks also go to Sinisa for helping with binding and for sharing Matlab code.

In addition to the contributions from my academic collaborators, this work would certainly have not been possible without the continued support from my family and friends. I owe my mom, Janet, many many thanks for her English expertise and for helping to edit the manuscript. I am also eternally grateful to my girlfriend Pengpeng for her encouragement and patience and for keeping me well fed during the writing phase. To my Grandparents Sally, Jim, and Barbara, I am grateful for your support and for always coming to visit when really it should have been the other way around. Also thanks to Leonard for his talents in space management: you can truly work miracles. To Uncle Steve, thank you for always being there and for reminding me to stick my head outdoors once in a while. Finally, much appreciation goes to little Geoffy for the always entertaining conversations and for keeping me on my toes.

Table of Contents

List of Tables

List of Figures

List of Abbreviations

AC	alternating current
AMPA	α-amino-3-hydroxyl-5-methyl-4-isoxazole-propionate
ap	apical dendrites
bas	basal dendrites
CNT	channel number tracking
CST	channel state tracking
exp	experimental result
GABA	gamma-Aminobutyric acid
ion	in graphs, refers specifically to voltage-gated ion channels
IQR	inner quartile range
mod	model result
mrkv	Markov
ms	milliseconds
mV	millivolts
nbins	number of bins
NLA	noise-like activity
NMDA	N-methyl-D-aspartic acid
nml	normal (0.35 Hz) postsynaptic potential firing rate
ODE	ordinary differential equation
onlyion	recording with voltage-gated ion channels active and synapses blocked
PDF	probability density function
PSD	power spectral density
PSP	postsynaptic potential
slow	slow (0.15 Hz) postsynaptic potential firing rate
stdev	standard deviation
syn	refers specifically to ligand-gated synapses
TEA	tetraethylammonium
trad	traditional
TTX	tetrodotoxin

Chapter 1

Introduction and Motivation

While the study of membrane potential fluctuations dates back to before Hodgkin and Huxley's seminal 1952 work on the squid axon,[1] the objectives of these studies have changed considerably and have recently entered a state of renewed of interest. Initially, ion channel fluctuations were studied because they provide detailed information about the workings of individual ion channels, providing much more information than could be obtained by simply studying the averaged behaviours of large channel populations.[2]

Recently, however, the advent of both increasingly powerful computers and new computational techniques[3],[4],[5],[6],[7] have made it possible to model large populations of ion channels. Likewise, there has been a growing realization that subthreshold fluctuations, or noise-like activity (NLA), plays important roles in the nervous system's function, beyond simply limiting the transfer of information.[8] For example, through the phenomenon of stochastic resonance, neuronal noise can enhance the transmission of weak periodic signals and aids in the detection of subthreshold signals.[9],[10], Additionally, it was recently proposed that neural noise could play a role in dynamical diseases, such as epilepsy, by providing the necessary impulse to push the brain from a normal state into a seizing state.[11]

While highly detailed models exist for individual neural elements acting as noise sources (henceforth noise generating elements), little is known about how these sources behave and

interact to generate the noise-like activity witnessed in large *in vivo* and *in vitro* systems, such as neurons or networks of neurons. Due to their inherent complexity, these systems are often difficult to study experimentally, where techniques are limited to application of blockers, drugs, and dynamic clamps. Therefore, experimental studies often benefit greatly from the micro-manipulations that can, at present, only be performed using computer models.

The purpose of this thesis is to isolate and examine the role that synapses play in contributing to noise-like activity in the neuron. Specifically, it will attempt to answer the question: do subthreshold oscillations arising from synaptic activity mainly result from the fluctuations of individual synaptic channels, or do they occur as a result of the synaptic response network activity? This question is of interest because a recent study has shown that certain measures of complexity decrease as a result of increased synaptic and/or gap junction activity.[12] This indicates that synapses could deliver low complexity input to the cell that could potentially carry information about the surrounding network. Thus, an answer to the question posed above is needed to determine whether synapses could indeed play such a role, or whether synaptic subthreshold input arises primarily from fluctuations within the synapse itself. We have taken a modeling approach because, at present, there are no experimental techniques for removing ion channel fluctuations without affecting other aspects of the system.

As a byproduct of our investigations, we provide two additional interesting findings. First, we provide experimental evidence indicating that synaptic noise in whole-intact hippocampal interneurons has a low frequency component, contrary to what was previously reported from pyramidal neurons in slice experiments. We then show using our biophysical model that fast synaptic activity, such as AMPA synapses, cannot replicate this behaviour but it can be easily explained by the addition of slow synapses such as NMDA and GABA_B. Secondly, we have developed a unique algorithm for fine-tuning our model by identifying statistical measures that relate to model parameters.

To summarize the contents of this document, first, a concise review of the relevant literature and a formal hypothesis is provided in this chapter. Chapter 2 provides an overview of the experimental and theoretical methods used in this paper. Chapter 3 presents the results, and

Chapter 4 discusses the implications.

1.1 Stochasticity in the Literature

This section provides an overview of the state of the art in studying large stochastic neural systems using stochastic elements. We begin by identifying prominent noise generating elements, such as voltage-gated and ligand-gated channels. Then, we present several recent studies that explain how many stochastic elements are incorporated into unified systems.

1.1.1 Sources of Neuronal Noise

Neurons are highly complex systems that rely on many components all working in unison. One function of these components is to create a potential across the cell's membrane and, in the case of excitable cells, generate action potentials. However, as in all physical systems, these components are subject to noise.

1.1.1.1 Fundamental Noise Sources

From fundamental physics, one can expect at least three sources of noise to be common to all neural and muscular systems: thermal noise, shot noise, and flicker noise.[2] The bulk of this work is focused on conductance fluctuations, but we will provide a brief review of the other types here. Thermal noise, also known as Johnson-Nyquist noise, is caused by the inherent thermal motion of charge carriers and provides information about the passive impedance of the membrane. Shot noise results from the fact that charge flows through the membrane in quantized units rather than as a continuous flow. Flicker noise is characterized by a 1/f spectrum and, although the precise physical basis in neurons is not clear, it has been observed in several physiological systems, such as the frog node.[13]

1.1.1.2 Noise Generating Elements

In addition to these fundamental noise sources, there are several specific neural elements that contribute to the generation of noise in the cell. The most common and widely studied are ion channel fluctuations. Ion channels are small yet active proteins that produce deterministic-like

behaviour in bulk quantities but, individually, have been shown under patch-clamp to fluctuate rapidly between open and closed states.[2][14] While these ion channels are responsible for deterministic-like behaviour, such as action potentials and the establishment of the resting membrane potential, they also introduce stochasticity into the system via two means. First, random opening and closing of the channel yields conductance fluctuations in the membrane that contributes to a major portion of the subthreshold NLA.[15] Secondly, the movement of the individual channel gates (structures in the protein that drive its opening and closing) also act to inject small randomly fluctuating currents into the cell. These currents, called gating currents, arise because the moving gates carry charged amino acid residues (generally part of the channel's voltage sensor). Although these currents are small, they can be detected and quantified using patch-clamping techniques.[16],[17]

In addition to channel fluctuations, there are several other sources of noise in neurons. Subthreshold NLA produced by ephaptic coupling refers to changes in membrane potential that are brought about by electric fields,[8] which could be particularly potent *in vivo*.[18] Similarly, gap junctions can carry both noise and information from nearby neurons and contribute to neuronal subthreshold oscillations.[12] Spontaneous postsynaptic potentials generated by ligand-gated ion channels are a major contributor and have been a major focus of work by Stacey *et al* and also Jacobson *et al*.[19][9][20] However, to the best of our knowledge, there has been no attempt to study the contribution of these channel's conductance fluctuations to subthreshold noise-like activity.[21]

It is clear that a great many noise sources combine to produce subthreshold fluctuations with specific properties. As will be demonstrated later, this is evident based on specific balances that must exist between the sources. However, for the purposes of modeling, it is necessary to make simplifications. Diba *et al*[15] and Jacobson *et al*[20] have identified voltage-gated ion channel conductance fluctuations and spontaneous postsynaptic potentials as being major components of subthreshold oscillations. Therefore, in this thesis we will elaborate on the roles of these noise sources in hippocampal interneurons and, at the same time, investigate the role of ligand-gated synaptic channel fluctuations, which have not been studied in this context up until now. For future reference, we will use the phrase ion channel fluctuations to refer specifically to

voltage-gated ion channel fluctuations and synaptic channel fluctuations to refer to the random opening and closing of synaptic ligand-gated ion channels.

1.1.2 Roles of Noise Generating Elements in Neural Noise

Presently, a considerable amount is known about how voltage-gated ion channels and spontaneous postsynaptic potentials contribute to subthreshold NLA. Diba *et al*[15] have performed a thorough study on ion channel fluctuations in cultured hippocampal neurons and have quantified the contributions from specific ion channels.

First, looking at raw noise amplitudes, Diba *et al* applied 4 blockers: including tetrodotoxin (TTX), a sodium channel blocker; tetraethylammonium (TEA), a non-specific potassium channel blocker; 4-aminopyridine (4-AP), a fast potassium channel blocker; and finally the L-type calcium channel blocker nifedipine. They also attempted to block all K^+ channels (fast and slow), by using a technique that allowed them to replace intracellular K^+ with Cs^{2+}. Sequential application of these blockers allowed them to rank various ion channels in terms of their contribution to subthreshold noise and showed that both sodium and slow Ca^{2+}-dependent potassium channels were strong contributors to subthreshold noise. Fast K^+ channels, however, were practically negligible due to their fast kinetics and small conductances.

Secondly, they examined the noise frequency spectrum and showed that, in most cases, current power spectral densities (PSDs) can be fit to the following equation, which is a Lorentzian when n=2:

$$S = \frac{A}{1 + \left(\frac{f}{f_c}\right)^n} \tag{1.1}$$

We will refer to this equation as the generalized Lorentzian. Furthermore, theory predicts that

for a channel fluctuating between open and closed states (Equation 1.2), n should equal 2.[15]

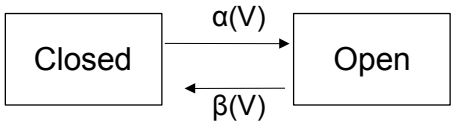

(1.2)

Finally, they demonstrated, that when multiple channels interact within in a single system, the PSD is well fit by Equation 1.1 and, more generally, can be represented by the sum of several Lorentzians. Experimental measurements on a sample cell gave a value of approximately n_v = 2.4 and f_c = 5Hz when averaged over several holding potentials.

The work of Jacobson *et al*[20] expanded on this analysis by studying the effects of input impedance. The input impedance was measured by injecting a 5-second-long 0.1Hz-100Hz chirp and measuring its voltage response. It is defined as the ratio of the Fourier transforms of these two signals, as shown below:

$$Z_{input}(f) = V_{output}(f) / I_{input}(f) \tag{1.3}$$

Using this, it became possible to measure how the random currents injected by channel fluctuations affect the membrane potential. They showed using TTX and synaptic blockers that a large portion of the sodium channel contribution to voltage noise comes not from the channel fluctuations themselves, but because of sodium's contribution to low frequency input impedance. For example, when stepping from -75mV to -55mV the voltage noise standard deviation increased 2.84 times, and 70% of this contribution was attributed to impedance increase in the low frequency range of 0.2-2Hz.

They also examined the effects of synaptic activity and showed that spontaneous postsynaptic potentials (PSPs) contributed mainly to the 5-100Hz frequency range, and had little effect on the lower frequencies and the input impedance. They attributed most of their synaptic activity to AMPA receptors, however, as we shall demonstrate, other types of synaptic receptors may play important roles as well.

Finally, the work of Serletis *et al*[12] has analysed synaptic, gap junction and ion channel noise from the point of view of complexity. They have shown that the addition of synaptic and/or gap junction blockers causes the complexity of the signal to increase and the log-log slope of the power spectral density to decrease, suggesting the subthreshold NLA becomes more complex (and likely stochastic) as the cell is isolated from the surrounding network. Conversely, this indicates that the presence of synaptic and/or gap junction activity should reduce complexity, thus implicating synapses as a source of low-complexity input that could potentially carry information about the surrounding network.

1.2 Hypothesis

We hypothesize that synaptic response to network activity should have a much greater effect on subthreshold NLA than the noise associated with synaptic channel fluctuations. As discussed above, this hypothesis is guided by the results of our colleagues Serletis *et al*[12], who show that complexity measures are reduced in the presence of synaptic activity; this indicates thats the low complexity synaptic responses to presynaptic network activity dominate over channel fluctuations, which are generally associated with high complexity.

To test this hypothesis, we have built a biophysically realistic model with synapses that can switch between Markovian (fluctuating) and traditional (non-fluctuating) formalisms. Switching the model between these two modes should capture the contribution of synaptic channel fluctuations. If our hypothesis is indeed correct, the changes in model output as a result of placing the channels in Markovian mode should be much less than the changes due to the initial introduction of traditional synapses. In order to quantify changes in model output, we examine raw traces, power spectral densities, and statistical measures.

Chapter 2

Methods: Experimental, Simulation and Analysis

We have obtained experimental recordings from hippocampal interneurons before and after the application of synaptic blockers. Our approach in this study was to use these recordings to validate a biophysically realistic model containing Markovian synaptic channels. Once we have confirmed that our model corresponds to physiological data by subjecting its output to a series of comparisons, we then switch the synaptic channels in the model between Markovian and traditional firing modes and statistically quantify the effects of this change.

2.1 Collection of Experimental Data

Experimental data were collected independently and described in detail by Serletis *et al*[12], but a summary of the relevant parameters is presented here. Whole-intact hippocampal tissue was obtained from C57/BL mice (P10-14) and stored in artificial cerebrospinal fluid (ACSF) composed of 123 NaCl, 2.5 KCl, 1.5 CaCl2, 2 MgSO4, 25 NaHCO3, 1.2 NaH2PO4 and 25 glucose (pH 7.4; all other units in mM). Tissue was incubated in a room-temperature ACSF bath for 1 hour prior to recording.

Recordings were acquired by applying whole-cell patch-clamps (2.4 GΩ seal) to fast-spiking stratum oriens interneurons of the CA3 hippocampal region. A Digidata 1322A was used for analog to digital conversion, while the Axopatch 200B amplifier acquired the recordings and applied the current clamp. Using the Clampfit 9.2 software, data were sampled and stored at 10 kHz, after low-pass filtering through an 8-pole 10kHz Bessel filter. The hyperpolarizing current was clamped to hold the resting membrane potential between -65mV and -60mV.

For each cell, four data traces were acquired according to the following algorithm:

1. Obtain clamp under ACSF perfusion
2. Measure I-V characteristics using a standard set of current pulses (100pA, 900ms duration, 50pA increments)
3. Record for 5 minutes. The first four minutes are used to ensure equilibration, and only the last minute is used for subsequent analysis
4. Re-measure I-V characteristics to assess stability of recording
5. Inject 0.4 seconds of 1nA amplitude Gaussian white noise
6. Switch to perfusion including gap junction blocker (1-octanol) and repeat steps 2-5
7. Switch to perfusion including both gap junction and synaptic blockers (1-octanol, CNQX, APV, and gabazine). Repeat steps 2-5
8. Washout with ACSF and repeat steps 2-5
9. Finally, to serve as a control, extracellular recordings were obtained by suspending the electrode outside of the cell. This represents contributions from ambient and synaptic noise

While we have described the complete experimental procedure, we did not make use of all of the noise response traces. Nor did we make use of the recordings done in ACSF solution.

2.2 Markovian Kinetic Models

While there are many viable models for fluctuating ion channels, there is often a trade-off between accuracy and ease of implementation. Markov models have been shown to address some of the limitations of the Hodgkin-Huxley model,[5] while at the same time being versatile enough to represent a wide range of channels. A common alternate approach to the Markov model is the approximate algorithm proposed by Fox et al[6] which, while it benefits from faster computation times, it diverges from expected results in certain scenarios.[3],[7]

2.2.1 Sodium Channel Markov Kinetic Model

In this section, we provide an example of how a channel's Markov representation is derived from its Hodgkin-Huxley-type ordinary differential equations. This algorithm is used to obtain Markov schemes for all voltage-gated and ligand-gated channels in this study; however we show the only sodium channel for purposes of brevity. Details of this approach are described by Strassberg *et al* and Mino *et al*[5],[3].

The traditional (Hodgkin-Huxley-type) equations that do not include channel fluctuations, as used by Traub *et al*,[22] are shown below for sodium channel current.

$$\begin{aligned} I_{Na} &= g_{max} \times m^2 \times h \times (V_m - E_{Na}) \\ \frac{\partial m}{\partial t} &= \alpha_m(V) \times (1-m) + \beta_m(V) \times m \\ \frac{\partial h}{\partial t} &= \alpha_h(V) \times (1-h) + \beta_h(V) \times h \end{aligned} \tag{2.1}$$

This is the standard form for describing a voltage-gated ion channel's conductance without accounting for channel fluctuations (see [14] for a reference). Note that, although m is commonly raised to the power 3 in axonal sodium channels, Traub *et al* use the power 2 for their somatic and proximal dendritic sodium channels.

In these equations, V is membrane voltage and E_{Na} is reversal potential, both in units mV. The variables I_{Na} and g_{max} are the channel current ($\mu A/cm^2$) and maximal conductance (mS/cm^2). The time-dependent variables m and h vary between 0 and 1 and represent activation and inactivation. The exponents of m and h represent the number of assumed gates of each type, in this case 2 and 1. Although not written out in the equations, m and h are both functions of time and voltage. The rate functions, α(V) and β(V), represent the rates of opening and closing of their respective gates. They depend on membrane voltage and are described below (in units ms^{-1}):

$$\alpha_m(V)=\frac{0.32*(13.1-V)}{\exp(\frac{(13.1-V)}{4})-1} \qquad \beta_m(V)=\frac{0.28*(V-40.1)}{\exp(\frac{(V-40.1)}{5})-1}$$
$$\alpha_h(V)=0.128\exp(\frac{17-V}{18}) \qquad \beta_h(V)=\frac{4}{1+\exp(\frac{40-V}{5})} \tag{2.2}$$

Using these equations, we can then represent each channel individually as a continuous-time discrete-state Markov process (sometimes referred to as a Markov jumping process).[3] First, since there are assumed to be two activation gates, we assign three states to this gate: zero open, one open, and two open. Likewise, for the one inactivation gate, we assign two states: open and closed. This gives a total of six states in the Markov kinetic model, as shown below. The rate constants describe the transition rates between states:

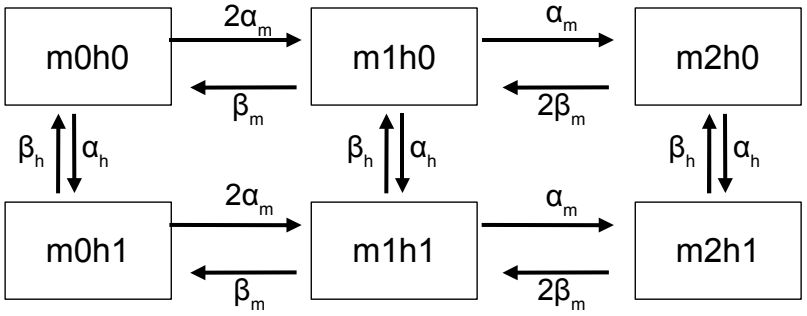

(2.3)

Since each channel is represented by its own jumping process and the open state is m2h1, the total conductance in a given compartment can be then expressed as follows:

$$I_{Na} = N_{m2h1} * \gamma_{Na} * (V - E_{Na}) \quad (2.4)$$

Here, γ_{Na} is the single channel conductance and N_{m2h1} is the total number of channels in state m2h1. The system is initiated with Nt channels distributed amongst the chain's states according to the chain's stationary distribution. Nt is generally estimated from the ratio $g_{max}*A_{compt}/\gamma_{Na}$,where γ_{Na} is measured experimentally and A_{compt} is the surface area of the compartment being modeled.

2.2.2 Implementation: Channel Number Tracking Algorithm

The standard way to implement Markovian ion channels in simulation is to track each channel's state individually, maintaining one complete Markov chain per ion channel in the model. For every iteration of the simulation clock, each Markov chain is updated according to its transition rates. This method is called a channel state tracking algorithm (CST) and, while suitable for single compartment models, it becomes cumbersome in large-scale simulations.

We and others have found that it is much more efficient to use a channel number tracking (CNT) algorithm, which keeps track of the number of channels in each state. Thus, only channels that are undergoing transitions need to be updated. A detailed comparison between these two methods is provided by Mino *et al*,[3] who showed that the two models give equivalent results.

Our comparisons, like Mino's, have found that the CNT algorithm is generally faster. However, we noticed that it gives the greatest performance boost compared to the CST algorithm when many channels spend long periods of time in a single state, or when transition times are slow compared to the simulation time step. In this situation, the CST algorithm continually tests each

channel for transitions that will never occur. Since the desensitized state(s) in kinetic models for ligand-gated synaptic channels generally have very slow exodus rates, CNT algorithms are particularly well suited. Conversely, however, when simulating channels that have fast transition rates relative to the simulation time step, CNT actually performs worse than the CST.

2.3 Simulation Environment

All equations were implemented within GENESIS[23] on an Intel Pentium computer running the Ubuntu Linux operating system, version 7.10.

Additionally, several customized GENESIS objects were developed for dealing with Markovian channels and will be available at the GENESIS website in the near future (http://genesis-sim.org/models). For a summary of these objects, see the Appendix.

2.4 Hippocampal Interneuron Model

In this paper, we use an interneuron model with a total of 51 compartments: 46 that form the soma and dendrite, 4 that make up the axon, and one axon initial segment.

Ionic channels and compartmental structure: Since we are incorporating both Markovian ion channels and Markovian synapses into a single model, it was necessary to utilize parameters from several sources. For the compartmental structure and ion channel parameters (conductances, channel kinetics, reversal potentials) we have duplicated the CA3 interneuron Traub *et al* proposed in their 1995 paper (henceforth the Traub model).[24] The compartmental structure and ion channel parameters remain completely unchanged, except that we have converted the traditional channels to Markovian channels as outlined in the previous chapter. Additionally, we shifted the sodium kinetics by +7mV to prevent spontaneous action potentials from occurring. The Markovian channels we implemented from the Traub model are the sodium

channel (Na); the high-voltage activated calcium channel (Ca); the delayed-rectifying potassium channel (K_DR); the A-type transient potassium channel (K_A); the calcium-dependent after-hyperpolarization channel (K_AHP); and the short-time voltage- and Ca-dependent potassium channel (K_C). See Table 1 for a summary of all channels implemented and their points of origin..

Additional non-synaptic noise sources: Unfortunately, we found that making the above ion channels Markovian was insufficient to account for the large level of noise present when both synaptic and gap junction blockers were in place. Therefore, we followed the approach used by Diba *et al* in 2002 (Diba model).[15] As reviewed above, they presented a highly detailed model of subthreshold noise generated by non-synaptic sources (mainly ion channels). To account for differences between model and experiment, they introduced both a potassium-permeable leak channel and also injected baseline noise. Therefore, we followed their approach and introduced an identical leak channel, except with a channel density of $0.004/\mu m^2$ ($1/3^{rd}$ their value). We also injected a similar baseline noise current with the following characteristics: zero mean; standard deviation of $3.00*10^{-12}$ amps ; power spectral density set to Equation 1.1 above, with f_c = 1 Hz and n=1; and random phase.

Synaptic inputs: AMPA, NMDA, GABA_A and GABA_B synaptic inputs are based on the network model proposed in the 1996 Traub paper[25] (Table 1). However, since we are representing subthreshold activity, we made several modifications. First, synaptic postsynaptic potential maximal conductances were scaled down dramatically: the conductance values we now use are more characteristic of unitary PSPs.[26] These values are $gmax_{AMPA}$ = 1000 pS; $gmax_{NMDA}$ = 51.3 pS; $gmax_{GABA\_A}$ = 368 pS; and $gmax_{GABA\_B}$ = 139 pS and were fine-tuned to match the experimental data. Our maximal conductance for NMDA is very small because we have already taken into account the magnesium blockage that is expected to occur at resting potential using the formula given in [27]. While this severely limits current inflow through NMDA channels, the channel's slow time constant and large electrochemical driving force allow it to still contribute significant depolarizations. Secondly, synaptic inputs were provided by the Genesis randomspike object, which approximates an exponential distribution of spiking events

when the simulation time step is much smaller than inverse mean firing rate. Note that we triggered paired AMPA and NMDA synapses in the same compartment by the same randomspike object, to ensure that they would fire together. The mean firing rate of each synapse was set to 0.35 Hz and the simulation time step was $2.5x10^{-5}$ seconds. Since there are 29 AMPA synapses firing at 0.35 Hz, this provides on average 10 AMPA PSPs per second, which is similar to the frequency for mini PSPs reported by Pare *et al*.[28] While this is twice the value used by Jacobson *et al*,[20] we found that it was necessary to replicate experimental parameters. Furthermore, Jacobson's value is based on a pyramidal cell model, and Traub's models have previously distinguished between interneurons and pyramidal cells in terms of synaptic noise rates.[25] We also made several other slight modifications to the network parameters that are summarized in the Appendix (Table 2). Most of these changes are present because we used code by Menne *et al*[29] for the basis of our model, and some of its parameters are slightly different from Traub's original paper.

Table 1: Summary of Simulated Channels

Traub 1996[25]	Diba 2002[15]	This thesis
Na	Na	Na_m (Traub version)
Ca		Ca_m
K_DR (fast)	K fast	K_DR_m (Traub version)
K_A		K_A_m
K_AHP (slow)	K slow	K_AHP_m (Traub version)
K_C		K_C_m
AMPA		AMPA_m
NMDA		NMDA_m
GABA_A		GABA_A_m
GABA_B		GABA_B_m
	Leak channel	Leak channel
	Injected current PSD	Injected current PSD

Channels used in this model are derived from two different sources, Traub 1996[25] and Diba 2002[15]. Suffix _m indicates our Markovian implementation.

Synaptic channel Markov schemes: Markov kinetic models for the synaptic channels are derived from two sources. First, models of NMDA, GABA_A, and GABA_B channels are based on those proposed in [27]. For the AMPA channel, we used a different model, since we found that when we implemented the channels in [27] the desensitization time was disproportionately long (Traub's model does not include desensitization at all). Thus, for the AMPA channel, we used the Markov scheme proposed by Stevens *et al.*[30] We also doubled all of the transition rates, since interneuron AMPA receptors have rise and decay times about twice as fast as those of pyramidal cells. For neurotransmitter release, we assumed a square pulse of 1 mM concentration and 1 ms duration.[27]

Neurotransmitter baseline concentration: In order to correctly simulate neurotransmitter concentration in the synaptic cleft in between release events, we estimated the steady state level of neurotransmitter from the formula provided in [31]. We assumed a resting presynaptic voltage of -60mV for pyramidal neurons and -45mV for interneurons, as reported by our experimental collaborator. While we included these estimates for completeness, and to avoid having the neurotransmitter concentration drop to absolute zero, we found that such low levels were insufficient to generate synaptic fluctuation in AMPA, NMDA, and GABA_B channels. GABA_A channels exhibited some fluctuations but, due to the low electrochemical driving force, the effects on membrane potential were minimal.

Single channel conductances: Single channel conductances were acquired from the literature. For voltage gated ion channels, we used the following values: sodium channel = 20 pS; delayed rectifying potassium = 10 pS; A-type transient potassium = 10pS; calcium-dependent after-hyperpolarization = 10pS; short-time voltage- and Ca-dependent potassium channel = 180pS.[15], [32] For synaptic channels, individual conductances are as follows: AMPA = 10 pS, NMDA = 45 pS, GABA_A = 20 pS, and GABA_B = 10 pS.[30],[33] While [33] has reported a single channel conductance as low as 5-6 pS for the K-channels coupled to GABA_B receptors, we have used the value of 10 pS to be consistent with the other K channels in our simulation.

2.5 Description and Justification of Statistical Quantities

We used several statistical measures in order to both tune our model's parameters and also to quantitatively compare the model's output to experimental data. In this section, we provide an overview of the statistical measures we used explain their purpose.

Standard deviation: A measure of the spread of the data. This was considered a measure of the amplitude of subthreshold fluctuations.

Skew: Represents the asymmetry of the data's distribution around the mean. Positive skew indicates that positive data points are more spread out on the positive side of the mean, and vice versa for negative skew. In our analysis, the skew is normalized to the standard deviation of the sample, and is used to represent the ratio between excitation and inhibition.

Kurtosis: Reflects how prone the dataset is to have data points lying beyond one standard deviation; high-kurtosis data appear graphically as data with many extreme departures from the mean. Gaussian distributed data has a kurtosis of 3. While some definitions of kurtosis subtract 3 to give gaussian data a kurtosis of zero, we did not use this convention. Generally, kurtosis was found to be a good measure of the ratio between fast (AMPA & GABA_A) and slow (NMDA and GABA_B) synaptic activity.

Power law scaling exponent: The power law exponent, β, is derived by fitting the following equation to a log-log plot of PSD, where A is a scaling constant and P(f) is spectral power:

$$\log(P(f)) = -\beta \log(f) + A \tag{2.5}$$

The scaling exponent is mainly used as a validation measure in order to ensure that the overall frequency spectrum is well represented. In the future, we will refer to the power law scaling exponents as beta estimates, or “betas” for short.

Spectral standard deviations: Spectral standard deviations reflect the square root power in specific frequency bands. We followed the definitions of Jacobson et al [20] for two of our bands: low (0.2-2Hz) and medium (5-100Hz). These bands are mainly used for purposes of comparison with Jacobson's work. We also introduced a high frequency band that ranges from 1kHz to 5kHz and is specifically designed to detect ion channel noise.

Probability distribution function exponent: This exponent, n, is derived from the sample's probability density function (PDF) or histogram, and is a measure of its gaussianity. It is described by the generalized Gaussian equation below, where A is a scaling constant, σ is standard deviation:

$$PDF = A * \exp\left(\frac{x}{\sigma}\right)^{n} \tag{2.6}$$

It is generally inversely related to kurtosis, but is more sensitive small deviations and aberrations in the probability density function. Therefore, we found it to be a good measure of our model's overall accuracy.

Correlation Dimension: The correlation dimension provides a characterization of the fractal dimension of a given trajectory in phase space.[34] It is estimated from the correlation integral, *C(l)*

$$C(l) = \lim_{N \to \infty} \frac{g}{N^2} \tag{2.7}$$

where g is the total number of points in phase space (constructed using Takens' method[35]) that have Euclidean distance less than l. This quantity estimates the fraction of points in phase space that are separated by distance less than l. Correlation dimension is then obtained by fitting the following equation to the linear region of a log-log plot of C and l:

$$\log(C(l)) \sim D_c \log(l) \tag{2.8}$$

Correlation dimension takes on low values when trajectories are generated by low-complexity deterministic-like systems, such oscillating networks of neurons. On the contrary, highly complex or stochastic processes, such as channel fluctuations, will generate large and theoretically infinite values of D_c. Therefore, D_c is often used to quantify the level of complexity

in a given signal.

2.6 Data Analysis Methods

Pre-processing: Initial data traces were all 60 seconds in length. For calculation of standard deviation, skew, kurtosis, PDF exponent, and correlation dimension, data were pre-processed as follows. AC spikes were identified in the datasets' PSDs using an automatic routine similar to that proposed by Zalay *et al*[36] and excised via notch filtering. Frequency components below 0.2 Hz were also removed by high pass filtering in Matlab (MathWorks, Natick MA) and cropping the first and last 3 seconds of data, resulting in 54 seconds of usable data.

Basic statistics: The statistics standard deviation, skew, and kurtosis were calculated by splitting the data into 5 second bins with 50% overlap and averaging over the trace.

PSD analysis: To obtain power spectral densities, data were divided into 5 second long Hann-windowed bins with 50% overlap. The PSD of each bin was averaged over the entire dataset. Betas were then measured as the slope of the best linear fit to the log-log plot of power spectral density. Data were fit in the range from 1 to 100 Hz.

PDF exponents: In order to calculate the probability density function (PDF) exponent, it was first necessary to derive the histogram. The appropriate number of bins was obtained based on the Freedman-Diaconis rule:

$$nbins = \left(\frac{max(x) - min(x)}{2 * IQR(x) * n^{\frac{-1}{3}}}\right) \tag{2.9}$$

In this formula, IQR is the inner quartile range of dataset x and n is the number of data points. In the event that nbins is non-integer, it is always rounded upwards. Then, the PDF exponent was

obtained by fitting the variable *n* in the generalized Gaussian distribution (equation 2.6) to the experimental data.

Spectral Standard Deviation: Spectral standard deviations are calculated by square rooting the summed the power values in the desired PSD frequency range.

Correlation Dimension: To calculate the correlation dimension, data were down sampled by a factor of 5 and then divided into non-overlapping bins of 1 second length. For each trace, only the first 40 seconds of data were used to reduce computation time, and since variances were small. Estimates of correlation dimension in each bin were averaged.

Averaging and error analysis: Once statistical measures are obtained for a given 60 second trace, these measures are averaged across multiple cells to obtain a population average. Experimental measures are averaged over 4 and 8 cells for the cases of only gap junction blockers and combined synaptic+gap junction blockade respectively. Model results are averaged over 3 trials with identical model parameters. Error bars represent the standard error across the population. We justify this because generally the cell to cell variation greatly exceeded than the variation between bins in individual datasets.

2.7 Algorithm for Tuning Model Parameters

While we used physiological estimates as the basis for as many of our parameters as possible, in some instances it was necessary to tune certain parameters using experimental data. This was mainly due either to the lack of knowledge about the physiology, or to the sensitivity of the model to the particular parameter.

The parameters we subject to fine tuning are synaptic PSP maximal conductances and synaptic firing rate. In our model, it was only necessary to tune AMPA, NMDA, and GABA_B maximal conductances, and we left GABA_A at its default value determined by Traub et al.

The following describes the statistics-based algorithm used to tune model parameters:

1. Initial parameter values were set to physiologically realistic estimates for firing rate and AMPA, GABA_A, NMDA, and GABA_B maximal conductances.
2. Firing rate was tuned to be the smallest value that allowed for significant visual overlap between the tails of NMDA and GABA_B PSPs. This was to ensure that there would be continuous tension between excitatory and inhibitory activity, which was necessary to generate the low-frequency oscillations witnessed experimentally (Figure 2).
3. We then ran the simulation with only NMDA synapses active and calculated the difference between the mean value and the minimum value of this data set. This gives the average depolarization produced by NMDA synapses. Then we repeated similarly for GABA_B, calculating the average hyperpolarization. The ratio of NMDA/GABA_B maximal conductances was then be scaled by the ratio (average hyperpolarization)/ (average depolarization). This allowed us to achieve the near-zero skewness that was present in experimental data.
4. While maintaining the new NMDA:GABA_B ratio obtained in step 3, we increased the maximal AMPA conductance until the correct kurtosis was reached.
5. After this adjustment, it was sometimes necessary to again tune the ratio of excitation (AMPA+NMDA) to inhibition (GABA_A/B) to achieve the correct skew. In most cases, however, it was not necessary since the experimental skew is slightly positive and the addition of AMPA synapses accounted for this.
6. Finally, we scaled all amplitudes until the correct standard deviation was achieved.

Chapter 3

Results

In accordance with our proposed procedure, we first present a detailed comparison between our model and the experimental results so as to validate our choice of model parameters. Secondly, we present a brief demonstration of how our model output is affected by the successive addition of AMPA, NMDA, and GABA_A/B type channels. Finally, we present a complete comparison of our model's output with and without synaptic channel fluctuations.

3.1 Validation of Model

This section serves to validate our choice of model parameters by demonstrating that the model accurately reproduces the raw outputs, power spectra, and statistical parameters of the experimental data. First, we present output traces with AC harmonics removed for both experimental and modeling results:

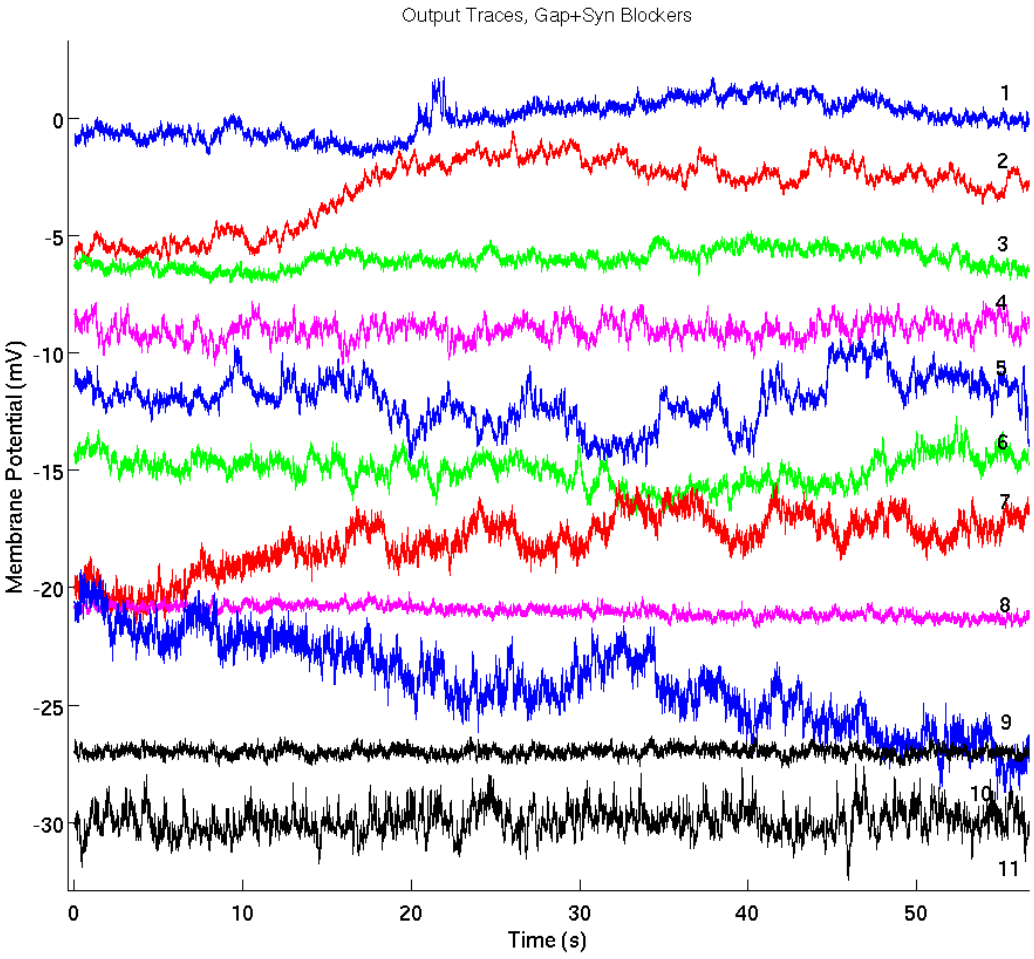

Figure 1: Experimental results, with all blockers

Traces 1-9 are experimental data (AC components removed) for the case where both synaptic and gap junction blockers are applied. Trace 10 is Markovian model output with only ionic channel activity. The bottom trace shows the Markovian model's output when synaptic activity is included. Trace 8 is disregarded from future statistical analysis.

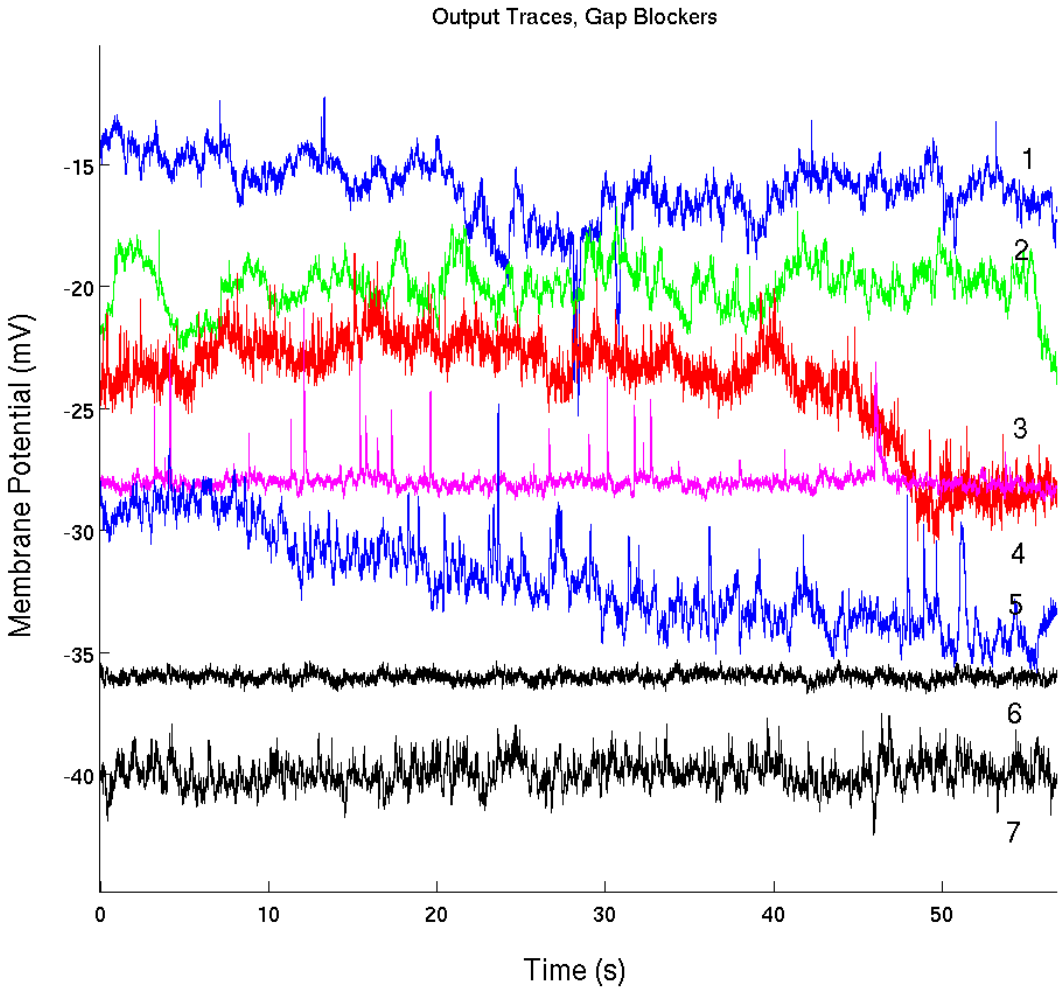

Figure 2: Experimental results, gap blockers only

Traces 1-5 are experimental data (AC componetns removed) for the case when only gap junction blockers are present. Trace 6 is model output with only ionic channel activity. The bottom trace shows the model's output when synaptic activity is included. Trace 4 is desregarded from future analysis.

We show these figures to illustrate that, qualitatively, model results look similar to our experimental data and to that presented elsewhere in the literature (see Figure 1 in [15] and Figure 3 in [20]). However, for our subsequent statistical analysis, we have excluded all recordings taken from cell #8 (trace 8 in Figure 1, trace 4 in Figure 2). This trace contains a number of EPSP spikes of very high amplitude, many over 6mV, that were rare in other traces. We justify this cell's removal because we do not believe one computer model can capture the diversity of all the interneurons of the hippocampus. While we have tried to model the average behaviour of the majority of the interneurons in our sample set, we believe that this particular cell would be

better represented by a modified model containing only AMPA synapses (as in [20]). Since only one out of the five cells we investigated has this appearance, we have chosen to omit it from the present analysis. In the future, a despiking algorithm could be used to remove the PSPs,[36] or it could be modeled separately after more similar traces are found.

Below are sample power spectral densities from a single cell with and without synaptic blockers, alongside the corresponding model output.

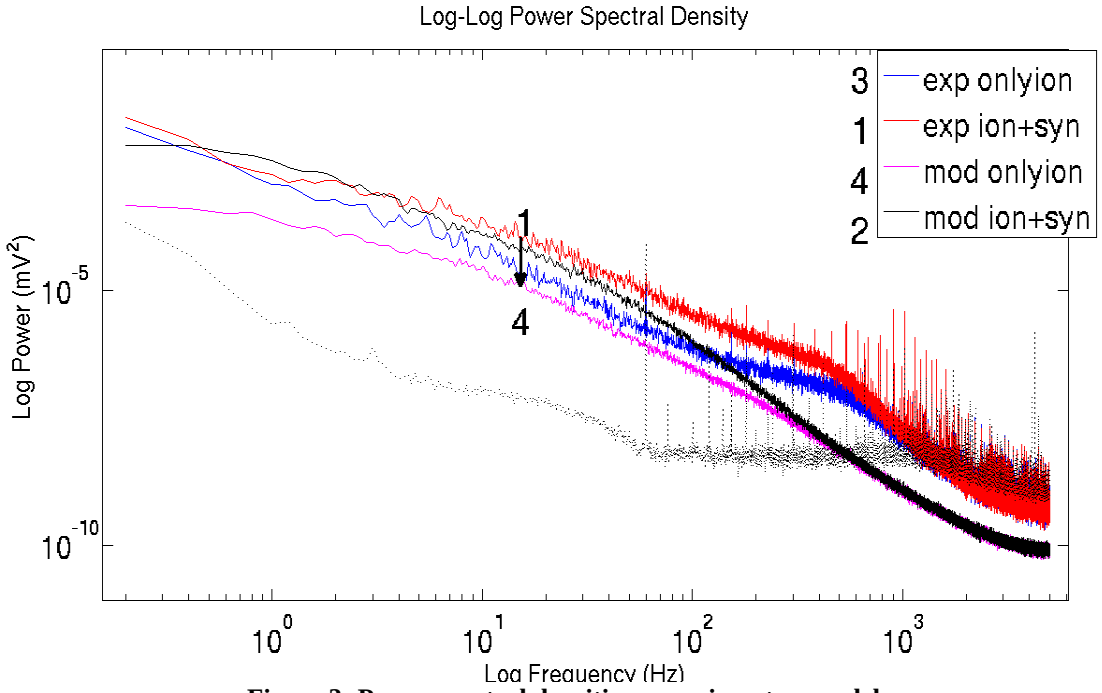

Figure 3: Power spectral densities, experiment vs model

Traces are labeled 1-4 from top to bottom at the location of the arrow. Traces 1 and 3 show the PSD of cell #7 without and with synaptic blockers, respectively. Traces 2 and 4 are for the Markov model under identical conditions. The dotted trace on the bottom shows extracellular ambient noise, which surpasses the signal at ~800 Hz. exp = experimental; mod = model with Markovian synapses and ion channels.

The power spectral density shows that, while there are similarities between the experimental and the model data, there are several features which the model cannot replicate. The experimental PSDs exhibit increased power in the range from 200-1000 Hz. This activity does not seem to come from the ambient noise and the model cannot account for it easily. It is most likely a non-synaptic phenomenon since it appears in traces with and without blockers. Since the focus of our

paper is on synaptic activity, and since its contribution to the total signal power is relatively small, we chose to disregard it and avoided measuring spectral standard deviations and betas from that region.

The following plots summarize the statistical analysis that was performed on the traces.

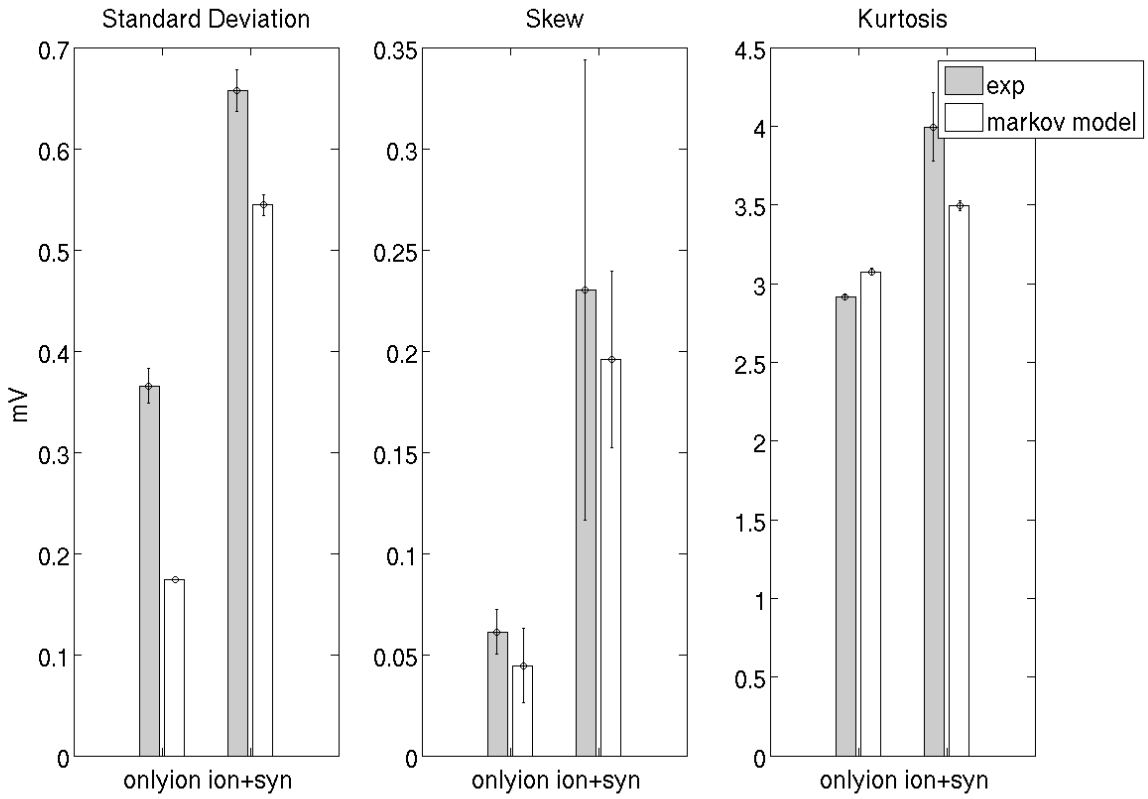

Figure 4: Basic statistics, experimental (shaded) vs model

Standard deviation, skew and kurtosis follow similar trends for both experiment and model. Skew and kurtosis values are closely aligned, but the model's standard deviation is reduced. Onlyion refers to recordings with only voltage-gated ion channels active and synapses blocked; ion+syn refers to recordings with both ion channels and synapses active. Shaded = experiment, unshaded = model with Markovian synapses and ion channels.

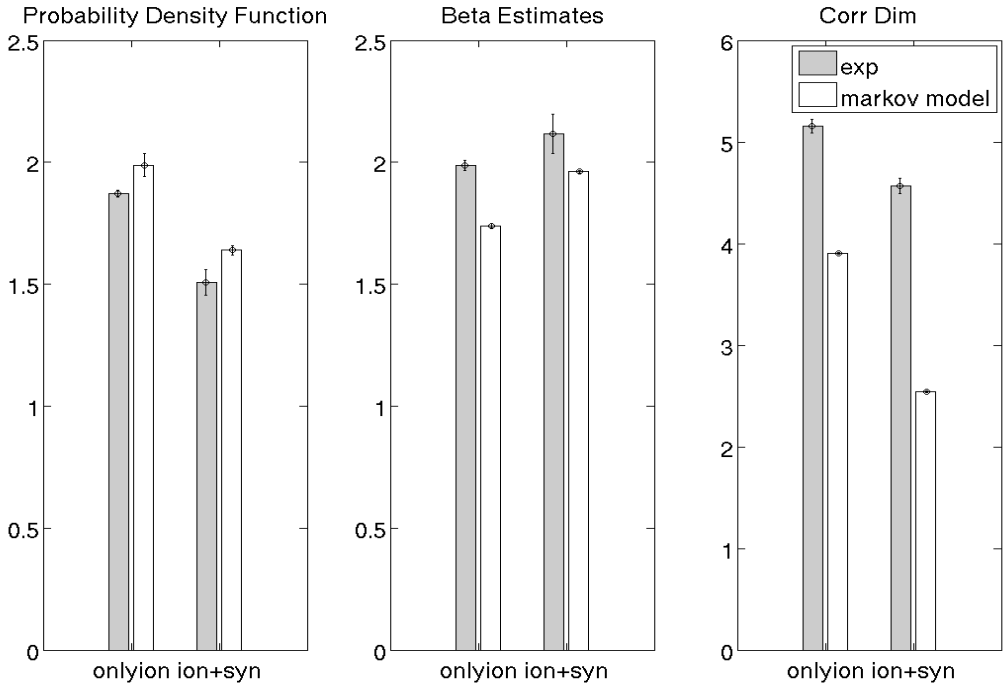

Figure 5: PDF exponent, PSD scaling exponent, and correlation dimension for experiment (shaded) vs model
Model reproduces experimental trends. Lower correlation dimension values for model can be explained by the presence of high frequency external noise in experimental output.

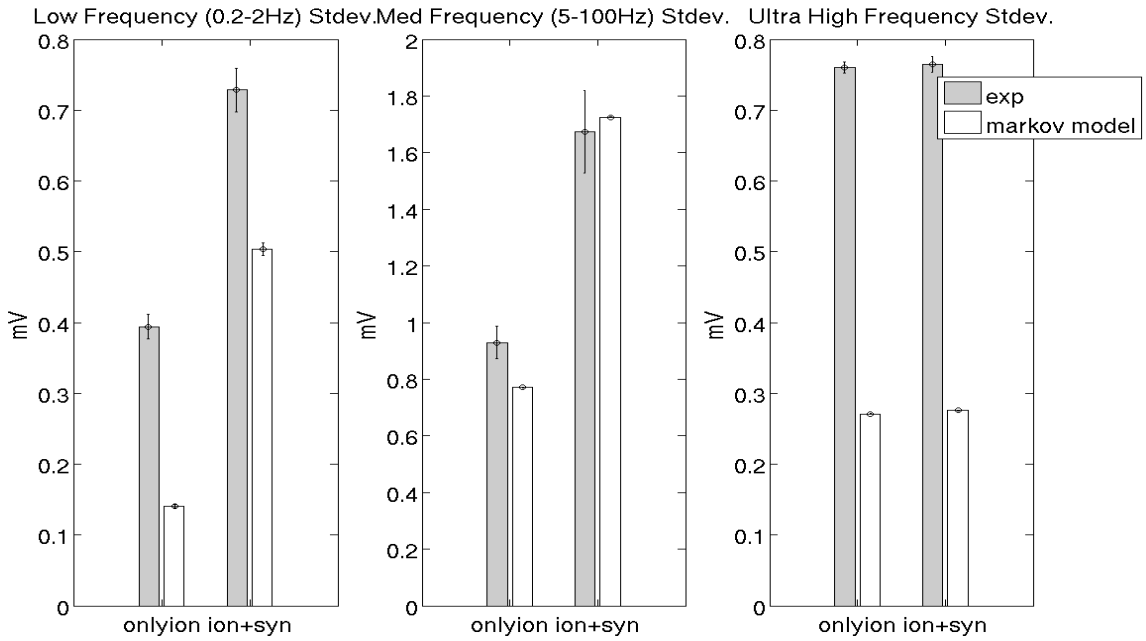

Figure 6: Frequency band standard deviations for experiment (shaded) vs model
Model replicates the experimental increase in both low and medium frequency noise following the removal of synaptic blockers. In the experiment, the majority of high frequency noise came from non-cellular (external) sources.

From Figures 4 to 6, it is clear that the statistics show a strong correspondence between experiment and model. In cases where the values don't match exactly, they still follow the same trends and the differences could be minimized by further fine-tuning model parameters.

The greatest difference between the experimental and model is the low frequency standard deviation statistic in Figure 6 for the case when only ion channels are active. This reflects an inability of the ion channels included in the model to replicate low frequency oscillations, which is also evident in Figures 1 and 3. We tried accounting for these oscillations several ways, including increasing the sodium channel density, shifting the channel kinetics, and increasing the concentration of slow calcium-dependent potassium channels. However, none of these strategies or the techniques implemented in [15] proved sufficient. While we could have adjusted the injected baseline noise PSD in order to account for this, it would have caused the injected noise to overwhelm the noise contribution of the ion channel fluctuations.

Possible sources of this low frequency noise are unblocked gap or synaptic junctions, field effects, voltage drift during recording, or any other sources of noise mentioned in Chapter 2. However, Diba *et al*[15] did not observe this low frequency component and reported a much lower standard deviation (0.19mV) for cultured hippocampal pyramidal cells at -60mV holding potential. Therefore it is possible that it is a unique feature of our experimental set up or cell choice.

3.2 Slow Oscillations and the role of NMDA/GABA_B Synapses

In Figure 6, experimental results show a significant decrease in low frequency noise when synaptic blockers are added. This indicates synaptic transients could make a significant contribution to the low frequency in interneurons from the whole-hippocampus, and is why we argue for the inclusion of synapses with slow time constants (NMDA and GABA_B) in the model.

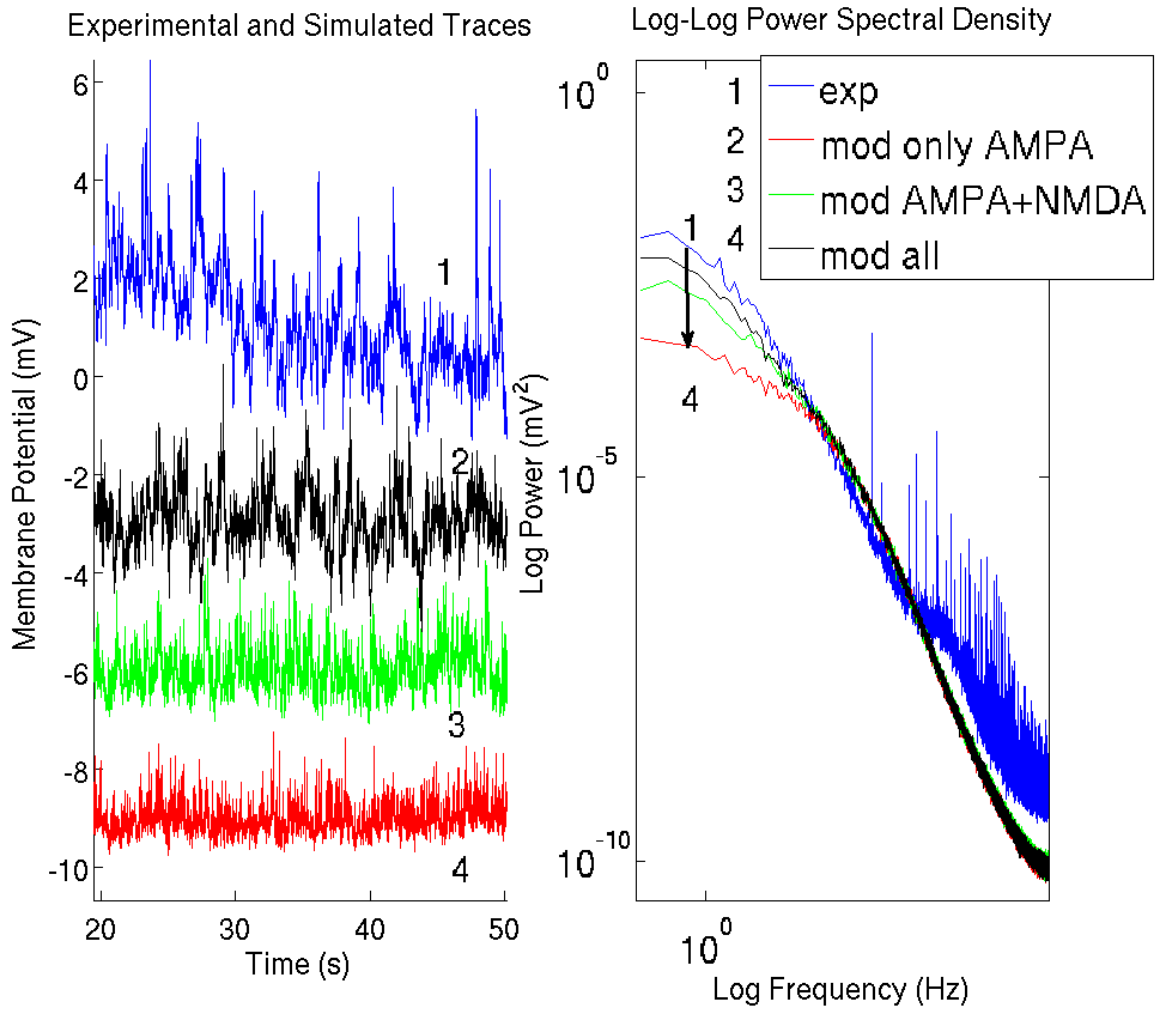

Figure 7: Output traces & PSD, effects of synaptic balance

Traces labeled 1-4 from top to bottom at location of arrow. The model output is shown with only AMPA synapses in Trace 4, and then the effects of adding NMDA (Trace 3) and GABA_A/B (Trace 2) are shown. In order to replicate the low frequency oscillations and the near-zero skew that exist under experimental conditions (Trace 1), it is necessary for a balance to exist between fast and slow synapses and also excitatory and inhibitory synapses. exp = experiment; mod = model with Markovian synapses and ion channels.

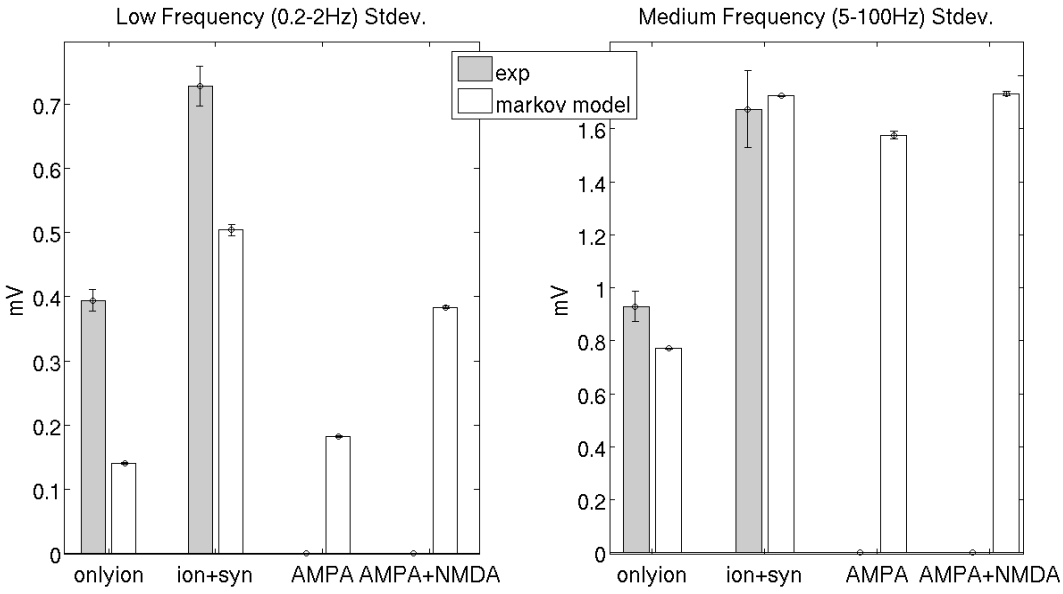

Figure 8: Effects of NMDA synapses on frequency bands

AMPA synapses alone do not contribute to low frequency oscillations, even though they can fully account for medium frequency activity. NMDA synapses allow the model to reproduce the synaptic component of low frequency oscillations. Shaded = experimental, unshaded = model with Markovian synapses and ion channels.

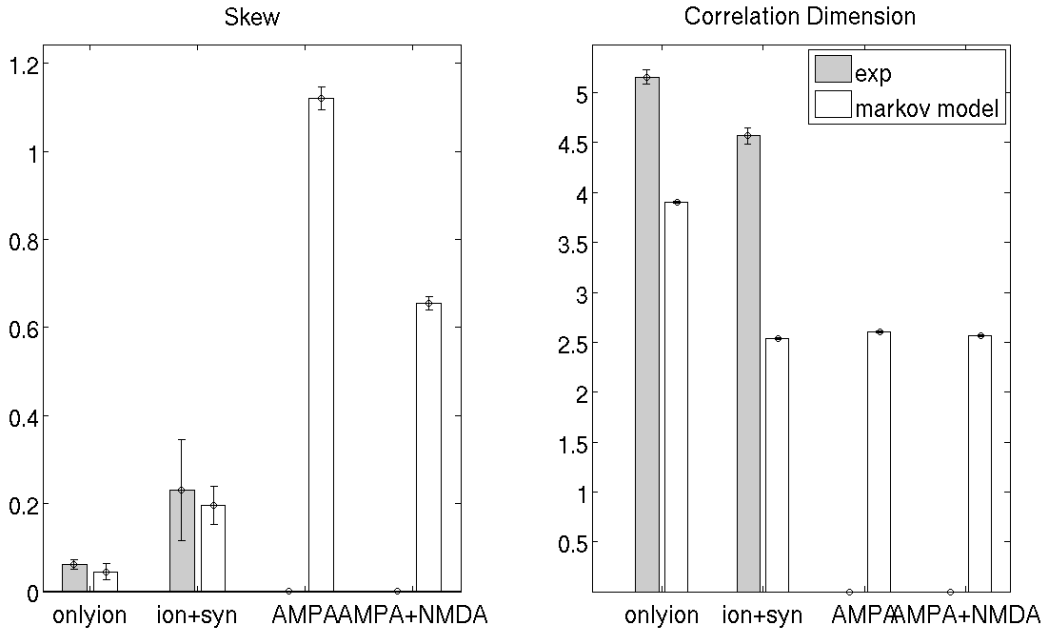

Figure 9: Effect of slow synapses on skew, and lack of effect on correlation dimension

Introducing AMPA and NMDA synapses of sufficient strength to account for the observed increase in frequency band standard deviation in Figure 8 resulted in unrealistic skew values. Correlation dimension remains unchanged. Shaded = experimental values, unshaded = model with Markovian synapses and ion channels.

The above figures compare the effects of adding various synaptic channel types to the model. Figure 7 illustrates qualitatively how the inclusion of additional synapse types allow for better simulation of experimental raw traces. The statistics support this: Figure 8 shows that our implementation of AMPA synapses cannot account for the increase in low frequency oscillations that are present experimentally. While the addition of NMDA synapses does significantly increase the low frequency contribution, without the presence of inhibitory synapses, the resultant data are highly skewed (Figure 9). Additionally, both the PSD and kurtosis measures are incorrect without the presence of slow synapses (not shown). Therefore, a balance between fast and slow synaptic action is necessary to correctly replicate the PSD and noise frequency bands, while a balance between excitation and inhibition is necessary to ensure correct skewness. While we acknowledge that it may be possible to obtain low frequency oscillations by specifically tweaking the parameters of our AMPA and GABA_A implementations, we found that this made it difficult to fit other statistics, and therefore the addition of slow channels was the simplest solution. We also note that, surprisingly, AMPA synapses alone can completely account for the drop in correlation dimension associated with synaptic activity, indicating they could dominate the low-complexity portion of the signal. In the future, each type of synaptic channel should be analysed individually for its effects on complexity.

3.3 Synaptic Channel Fluctuations

Finally, in this section, we will attempt to address the question of whether synaptic fluctuations contribute significantly to synaptic noise-like activity. The plots below show the effects of switching the synaptic channels from Markov to traditional modes.

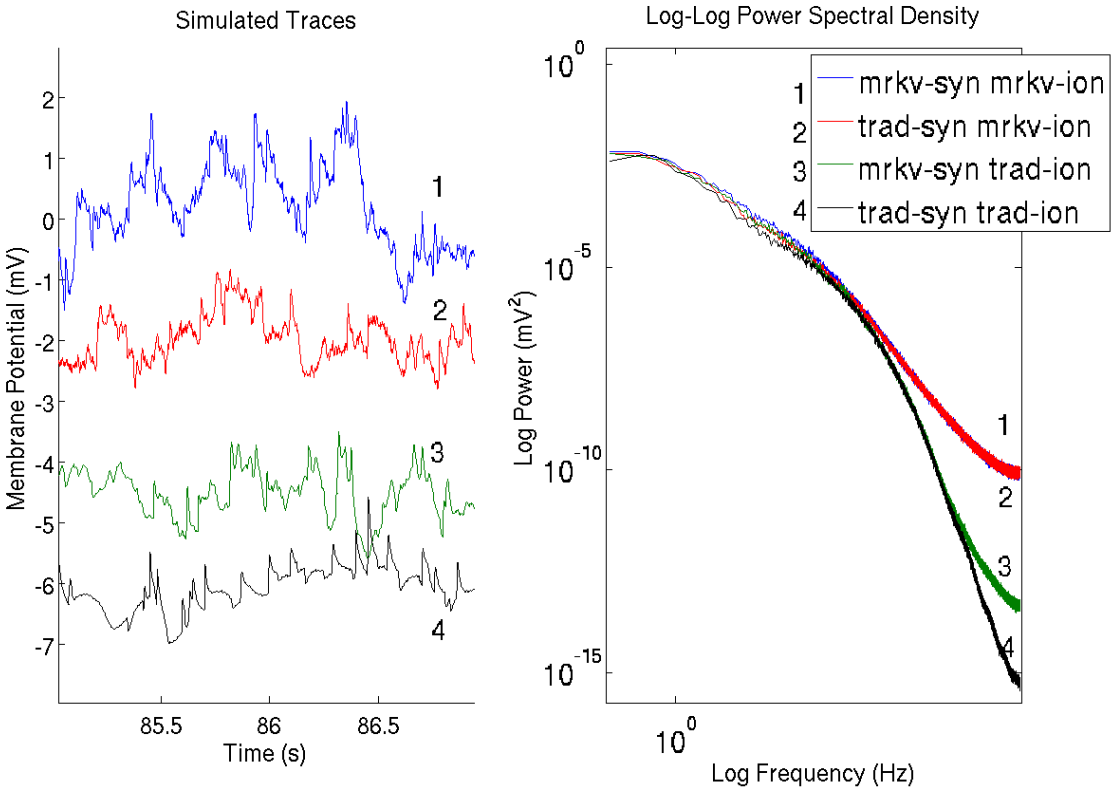

Figure 10: Effects of fluctuations, simulated traces and PSD

Markov vs traditional synapses when ion channels are Markovian (traces 1 & 2) show little discernible difference in raw traces. In PSD there is subtle difference in the 5-80Hz range. Comparing Markov and traditional synapses when ion channels are traditional HH-type (traces 3 & 4) shows qualitative differences in the raw traces, a substantial drop in high frequency PSD, and a drop in 5-80Hz PSD. mrkv=Markov; trad=traditional; syn=synapse.

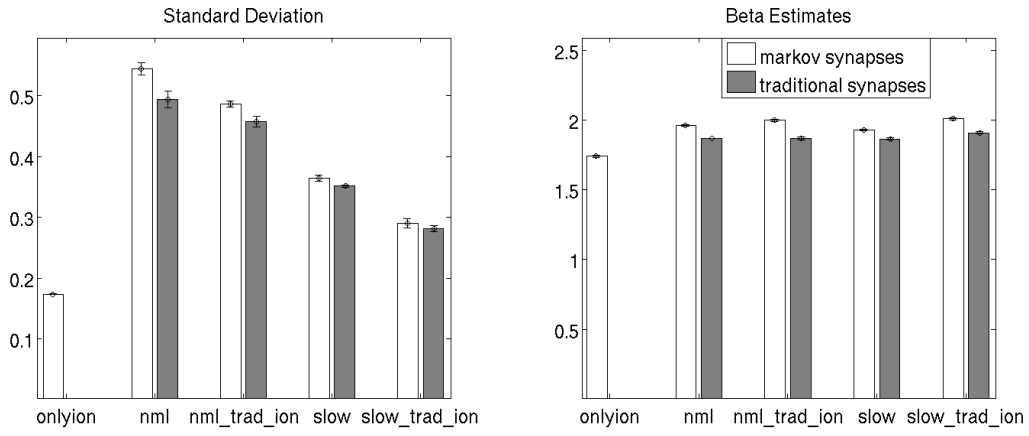

Figure 11: Effects of synaptic fluctuations on standard deviation and betas

Standard deviation drops in all cases when synapses are modelled traditionally. Likewise, the beta estimate (slope of log-log plot for 1-100Hz) drops perceptibly for traditional synapses, indicating that the power spectrum becomes more flat in this range. Abbreviation nml refers to simulation with 0.35Hz firing rate, and slow refers to simulation with 0.15 Hz firing rate. Trad ion refers to the when voltage-gated ion channels use the traditional HH formalism.

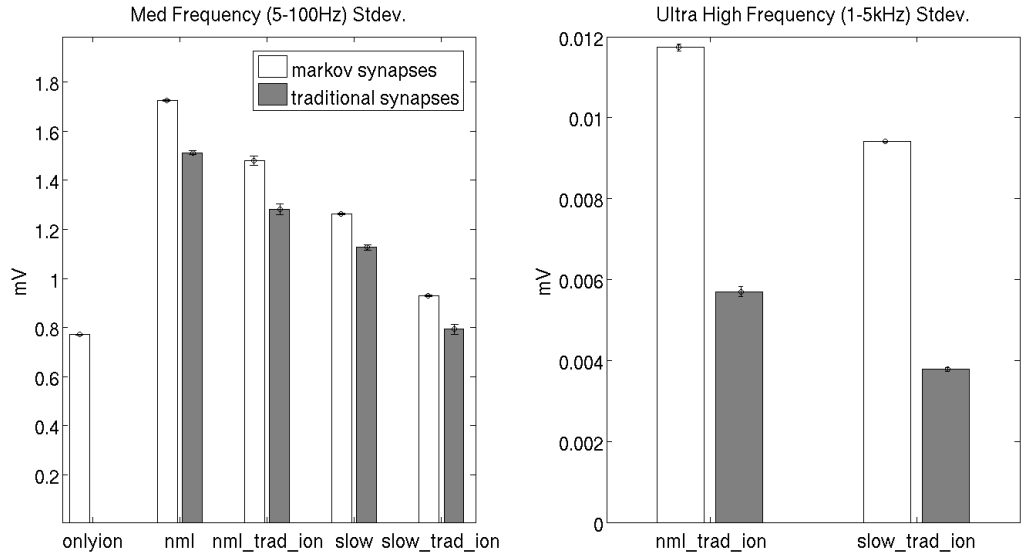

Figure 12: Effects of synaptic fluctuations on spectral standard deviations
Medium frequency is affected in all cases by synaptic fluctuation (left), whereas effects on high frequency are only perceptible in the case when ion channels are non-fluctuating. Abbreviation nml refers to the simulation with 0.35Hz firing rate, and slow refers to simulation with 0.15 Hz firing rate. Trad ion refers to the situation when voltage-gated ion channels use the traditional Hodgkin-Huxley formalism.

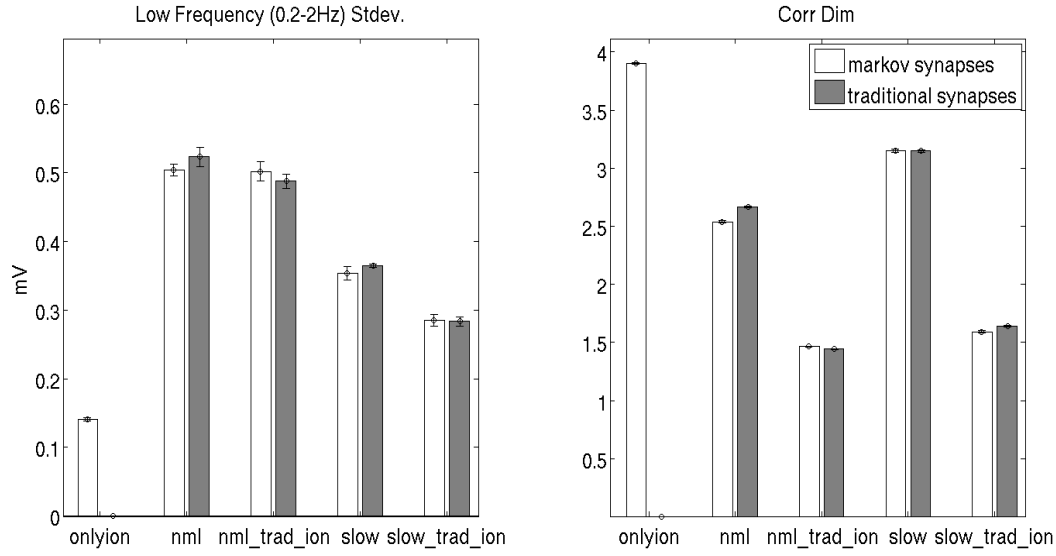

Figure 13: Lack of effects of synaptic fluctuations on low freq and correlation dimension
Comparison shows that the 0.2-2Hz range is relatively unaffected by synaptic fluctuations, and no consistent trend appears in correlation dimension estimates either. Abbreviation nml refers to simulation with 0.35Hz firing rate, and slow refers to simulation with 0.15 Hz firing rate. Trad ion refers to the situation when voltage-gated ion channels use the traditional Hodgkin-Huxley formalism.

From Figures 10, 11, and 12, it is clear that synaptic channel fluctuations are significant enough to alter many statistical properties of the output signal at the neuron's soma. From Figure 12, we

see that when voltage-gated ion channels are made non-fluctuating, over 50% of the synaptic high frequency noise is caused by synaptic channel fluctuations; these fluctuations appear in the raw traces and PSDs shown in Figure 10. Additionally, statistics such as standard deviation and beta estimates (Figures 11 and 12) are able to pick up the effects of synaptic channel noise over and above the noise from non-synaptic sources, indicating that synaptic channel noise should have statistically measurable effect in *in vitro* systems.

The experiments done using a slow firing rate (0.15Hz) and with traditional ion channels are designed to test robustness of our results to shifts in parameters and will be addressed in the discussion. We also tested the robustness of these results by using the model to measure subthreshold fluctuations at various locations throughout the cell. Specifically, we recorded from the most distal apical dendrites and the most distal basal dendrites (Figures 14 through 17).

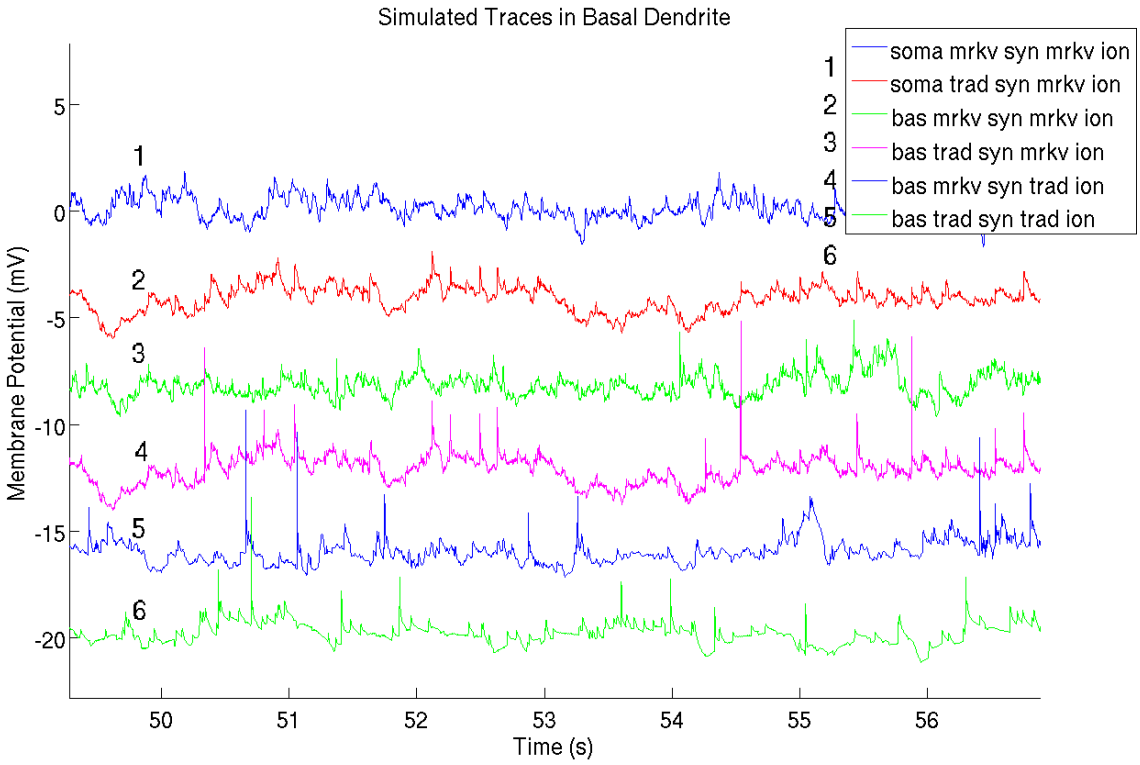

Figure 14: Synaptic fluctuations in basal dendrites, simulated traces

Due to small compartment size and lack of attenuation, synaptic channel noise is much stronger in basal compartments. The legend shows the location, nature of synapses [Markov or traditional], and nature of ion channels of traces going from top to bottom

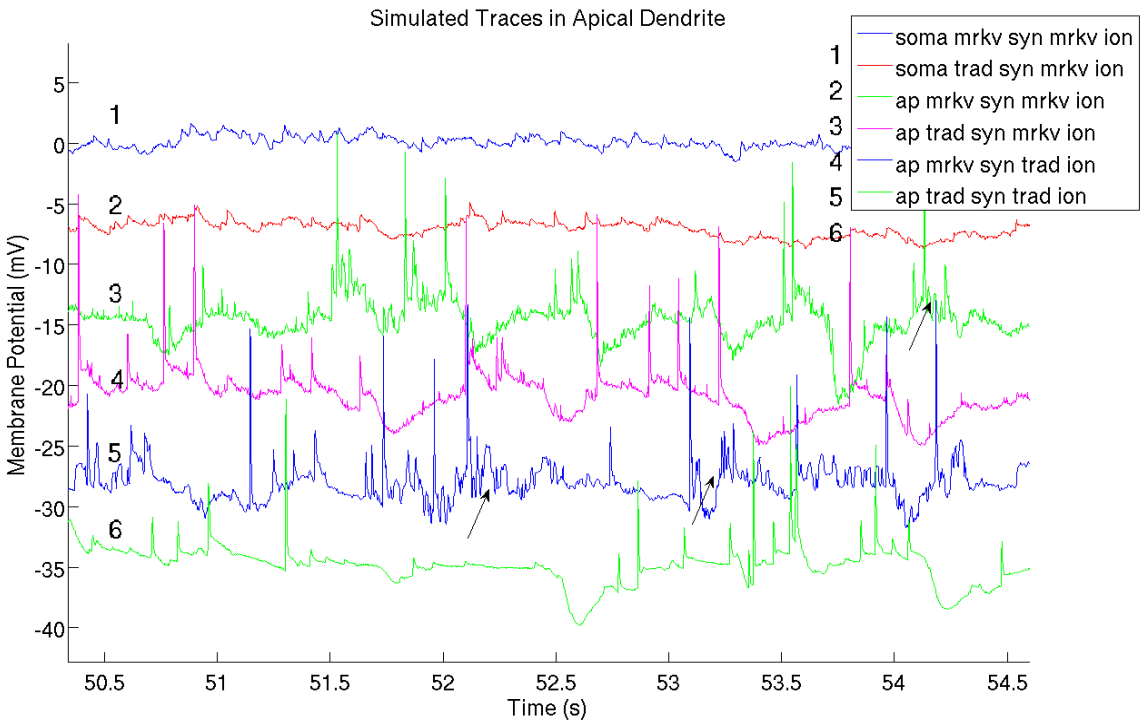

Figure 15: Synaptic fluctuations in the apical dendrites, simulated traces

Channel noise is also much stronger in apical dendrites. Arrows pointing to the ripples following AMPA PSPs indicate fluctuations of individual NMDA channels. The legend shows the location, nature of synapses [Markov or traditional], and nature of ion channels of traces going from top to bottom.

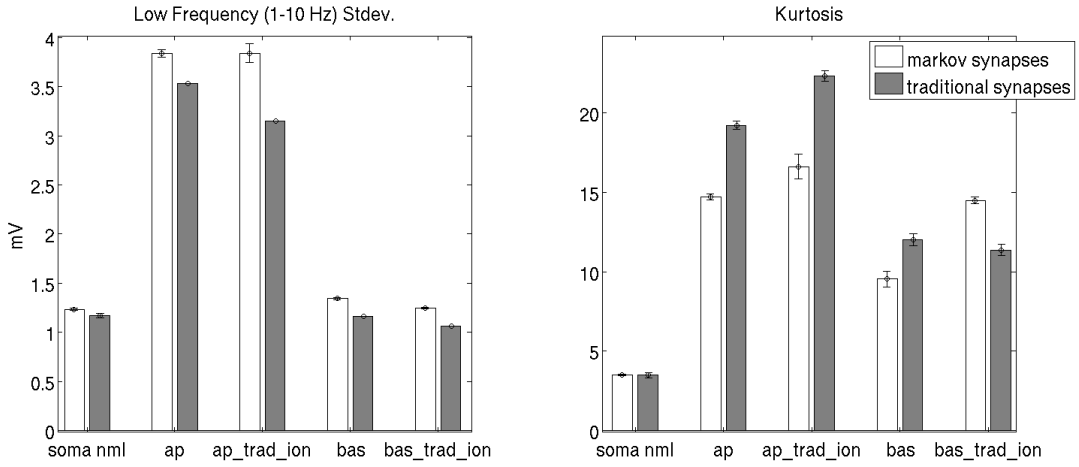

Figure 16: New statistical trends in dendrites as a result of synaptic fluctuations

Low frequency noise increases as a result of synaptic fluctuations, and kurtosis is also affected in a situation-dependent manner. ap = apical dendrites, bas = basal dendrites.

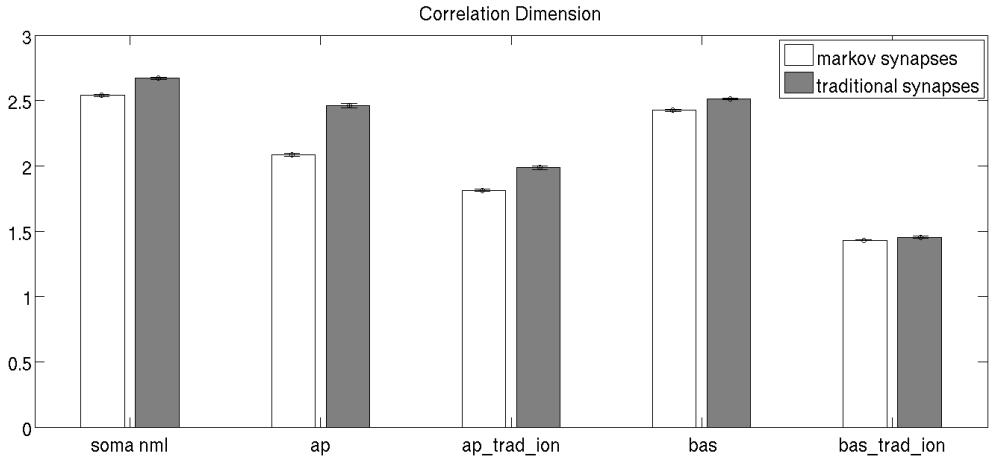

Figure 17: Synaptic channel fluctuations decrease correlation dimension in dendrites
In most instances, there is a significant increase in correlation dimension when traditional non-fluctuating synapses are used. Since we simulate synaptic inputs as stochastic poisson processes, this could reflect increased propagation of synaptic signals from other parts of the cell to the measured compartment.

The recordings in Figures 14 to 17 show that the effects of synaptic fluctuations became more pronounced in recordings from basal and apical dendrites. In some cases, individual opening and closing events of NMDA channels were clearly visible (Figure 15), which is likely a result of the small compartment size, large NMDA single-channel conductance, and strong electrochemical driving force. The standard deviation, beta estimates, and medium frequency and high frequency band oscillations all increased in the same manner as they did at the soma (not shown). Additionally, some new statistical trends appeared (Figures 16 & 17). The meaning of these trends will be addressed in the discussion. Unfortunately we lack experimental dendritic to serve as a comparison point for these results, and the implications of this will also be addressed in the discussion.

Chapter 4

Discussion

4.1 Sensitivity of Results to Shifts in Model Parameters

In Figures 11 through 17, the simulations with a slow firing rate (0.15 Hz) and traditional ion channels are designed to test the robustness of our results to extreme shifts in model parameters. For example, the 57% decrease in firing rate associated with the slow case does not cause the Markovian synapses to become significantly more or less pronounced.

Likewise, simulating the ion channels using the traditional, non-fluctuating formalism is analogous to setting the ratio of synaptic/non-synaptic noise-like activity to infinity. The effects of Markovian synapses do not appear any less pronounced when non-synaptic noise is present, as compared to when it is absent. Therefore, it would appear that other sources of noise within the cell do not significantly mask the noise contribution from synaptic channel fluctuations. The one exception to this, however, is the complete dominance of non-synaptic noise sources in the high frequency (1-5kHz) band (Figures 10 and 12).

Measuring synaptic noise-like activity in both the apical and basal dendrites showed similar statistical trends to those in the soma (not shown). This shows that synaptic channel fluctuations

have a ubiquitous effect throughout the cell.

4.2 Emergence of New Trends in Dendrites

Figures 16 and 17 highlight some of the new statistical trends that emerge when recordings are performed in the dendrites. The trends in Figures 16 result simply from the fact that the synaptic noise is much stronger closer to the source and, therefore, it has more influence over signal statistics. Particularly interesting, however, is the fact that correlation dimension in Figure 17 appears to increase when synapses are modelled traditionally. This is contrary to intuition, and should be investigated further. However, we hypothesize that this increase could result from the fact that we are using a stochastic process to drive synaptic PSPs. Therefore increased transmission of PSPs from neighbouring dendritic compartments and also backpropagation from the soma could potentially explain the heightened correlation dimension measure.

While these dendritic recordings are informative, we acknowledge that they are extrapolations based upon what we know of somatic activity and estimates of neuron geometry, and are therefore subject to inaccuracies. However, we justify their validity based on the fact that they are based on a reputable model for cell geometry.[24] Additionally, interneuronal dendrites tend to have short electrotonic lengths and hence low sensitivity to the precise location of synapses.[25] Therefore, our model should provide a fairly good qualitative approximation to the activity at the dendrites: namely the lack of attenuation and smaller compartment size provides a magnified version of the synaptic activity we observed at the soma and, likewise, an attenuated version of the somatic voltage-gated ion channel fluctuations.

4.3 Effects of synaptic channel fluctuations

Initially, we hypothesized that synaptic noise-like activity resulting from network activity should have a greater effect on subthreshold NLA than that resulting from synaptic channel fluctuations. We have prepared a model interneuron that matches averaged trends from experimental data (Figures 1 through 6). While we have observed ubiquitous effects of synaptic channel fluctuations throughout the neuron, it appears that the magnitude of the contribution

from these fluctuations is much less than the synaptic response to network activity. For example, in the Figure 11 standard deviation plot, the difference between the onlyion column and the shaded nml column (~0.32mV) is much greater than the difference between the unshaded and shaded nml columns (~0.05 mV). This shows that switching synapses from being traditional to being Markovian had a much weaker effect on standard deviation than did the initial introduction of traditional synapses. This same is true for the other statistics as well (Figures 10 to 12). This is not too unexpected, since a number of other studies have successfully accounted for synaptic activity in models without the of synaptic ion channel fluctuations.[20],[37]

There are several other factors that we have not taken into account and that could dramatically increase the contribution of synaptic channel fluctuations to NLA. First, our estimates of the baseline levels of transmitter in the synaptic cleft were extrapolated from model data, rather than being based directly on experimental evidence.[31] Since this model primarily dealt with representing transmitter responses to action potentials, it may not be very reliable for representing resting neurotransmitter concentrations. If the actual baseline values are even one order of magnitude higher, our preliminary investigations have shown that the baseline synaptic channel fluctuations could contribute significantly to NLA.

Additionally, synaptic channels located outside the synapse itself have recently received much attention in the academic community.[38] These channels respond to neurotransmitters that are released at a separate location and diffuse up to hundreds of micrometers to reach the channel. This diffusion is reflected by an extracellular ambient level of neurotransmitter that can be as high as 1μM.[39] This topic has been reviewed by Mody,[38] who reports that extrasynaptic GABA_A channels can present a “massive” tonic inhibition in hippocampal neurons. Since these receptors are gated by varying levels of neurotransmitter, their current fluctuations could introduce considerable noise into the system. In the future, we should investigate how these types of channels would be affected by the blockers Serletis *et al* have introduced.

Finally, noise due to synaptic channel fluctuations has the unique property that its existence depends on neurotransmitter release. It is plausible to hypothesize that synaptic noise levels

could therefore vary with time and be correlated with various external processes. Our model provides the ideal test bed for this hypothesis. Therefore, although the synaptic channel fluctuations appears to be weak, its time-varying properties may have significant impact on information transfer.

4.4 Synaptic contribution to low frequency oscillations

In Figures 7 through 9 we have shown experimental findings demonstrating that low frequency oscillations increase significantly as a result of synaptic activity. This is contrary to the *in vitro* findings of Jacobson *et al*[20] who have shown that synaptic noise mainly contributes to the 5-100 Hz band, and negligibly to the low frequencies. While this difference begs further investigation, it could potentially be a result of either our choice of cell type, or experimental set up, since Jacobson's group worked with neocortical interneurons in slices.

We have hypothesized, based on our modeling results, that this low frequency contribution is caused by slow synapses such as NMDA and GABA_B. This hypothesis is experimentally falsifiable, and could be tested by observing the effects of NMDA blockers on subthreshold noise *in vitro*. Indeed, experimental work is necessary to confirm or deny this hypothesis because low frequency oscillations can theoretically be generated by other synaptic means as well. For example, sufficiently fast firing of AMPA and GABA_A synapses, as seen in the detailed biophysical model of Destexhe *et al*,[37] generate low frequency behaviour. However, we should point out that, in our model, increasing the rate of firing had unrealistic side effects, implicating NMDA/GABA_B channels as the best and simplest solution.

Chapter 5

Conclusions

From the preceding statistical analysis, we can see that synaptic channel fluctuations have a) a ubiquitous effect throughout the cell and b) are insensitive to parameter shifts like firing rate. They can produce relevant effects on statistical measures, such as standard, deviation, power-law scaling exponent, and power spectral density in the 5-100 Hz and 1-5 kHz ranges. However, it is also apparent that synaptic channel fluctuations are significantly more subtle than synaptic response to network activity in terms of their raw amplitude, thus validating our initial hypothesis. Therefore, this indicates that synaptic subthreshold activity could indeed reflect external network behaviour.

We have also identified a secondary finding, that synaptic NLA contains a low frequency component that could be generated by the spontaneous activity of NMDA/GABA_B synapses. However, further studies are needed to a) quantify the contributions of individual synapse types, b) investigate the roles of baseline neurotransmitter concentrations and extrasynaptic channels, and c) demonstrate the exact relationship between model parameters and statistical measures.

Appendix

Changes to Synaptic Parameters from Traub 1996 Model

Table 2: Changes to Synaptic Parameters from Traub 1996 Model

Parameter	Traub 1996 version[25]	Version implemented in this thesis
Location of excitatory synapses	Located 175μm or more from the soma in long dendrites 75μm or more in short dendrites, NMDA and AMPA always occur together	Located in compartment levels 1, 8, 9, 10. NMDA and AMPA always occur together
Location of GABA_A synapses	Located in most proximal dendrites	Same (located in compartment levels 3 and 5)
Location of GABA_B synapses	Located in compartments > 240μm from soma	Located in compartments 9, 10, and 11
Number of excitatory synapses	33 AMPA & NMDA	29 AMPA & NMDA
Number of GABA_A synapses	96	43
Number of GABA_B synapses	10	23

List of Custom GENESIS Objects

New Objects:

GENvgpores - Voltage-gated ion channels with Markovian gating; supports variable numbers of gates (0-4 activating gates and 0-1 inactivating gates); HH-based rate constants

GENgap - 4-state gap junction with Markovian gating

GENsynpores - Generalized transmitter-gated synapses with Markovian gating

GENtabchan - Same as GENvgpores, but rate constants are based on tables

GEN_Gprotein - Markovian simulations of G-protein concentrations

Note: All of the above objects use the channel number tracking algorithm.

GENESIS functions for object manipulation:

stochastify - function to search through element trees and automatically convert traditional channels to Markovian channels (uses libraries)

volumeconnect_general - Generalized version of volumeconnect command to work with either traditional or Markovian synapses

create_markov_synapse - specialized function to automatically flip traditional synapses to Markovian synapses (can pass to volumeconnect_general)

gapconnect_general - Similar to volumeconnect_general, except for forming connecting gap junction connections

Bibliography

1: Hodgkin AL, & Huxley AF. A quantitative description of membrane current and its application to conduction and excitation in nerve. *J. Physiol.* **117**, 500-544 (1952).

2: Stevens CF. Inferences About Membrane Properties From Electrical Noise Measurements. *Biophysical Journal* **12**, 1028-1047 (1972).

3: Mino H, Rubinstein JT, & White JA. Comparison of Algorithms for the Simulation of Action Potentials with Stochastic Sodium Channels. *Annals of Biomedical Engineering* **30**, 578-587 (2002).

4: Chow CC, & White JA. Spontaneous action potentials due to channel fluctuations. *Biophys. J.* **71**, 3013-3021 (1996).

5: Strassberg AF, & DeFelice LJ. Limitations of the Hodgkin-Huxley formalism: Effects of single channel kinetics on transmembrane voltage dynamics. *Neural Comput.* **5**, 843-855 (1993).

6: Fox RF. Stochastic versions of the Hodgkin-Huxley equations. *Biophys. J* **72**, 2069-2074 (1997).

7: Bruce, I.C. Evaluation of Stochastic Differential Equation Approximation of Ion Channel Gating Models. *Ann. Biomedical Engineering* **37**, 824-838 (2009).

8: Faisal AA, Selen LP & Wolpert DM. Noise in the Nervous System. *Nature Reviews* **9**, 292-303 (2008).

9: Stacey WC, & Durand DM. Stochastic resonance improves signal detection in hippocampal CA1 neurons. *Journal of Neurophysiology* **83**, 1394-1402 (2000).

10: Stevens CF, & Zador AM. Input synchrony and the irregular firing of cortical neurons. *Nature Neurosci* **1**, 210-217 (1992).

11: Lopes da Silva FH, Blanes W, Kalitzin S, Parra J, Suffczynski P & Veils DN. Dynamical Diseases of Brain Systems: Different Routes to Epileptic Seizures. *IEEE Trans. on Biomedical Engineering* **50**, (2003).

12: Serletis D, Zalay OC, Valiante TA, Bardakjian BL, & Carlen PL. Complexity in cellular

noise-like activity in the nervous system. *Unpublished manuscript* , (2009).

13: Verveen AA, Derksen HE. Fluctuations in membrane potential of axons and the problem of coding. *Biological Cybernetics* **2**, 152-160 (1965).

14: Hille B. *Ionic Channels of Excitable Membranes* (Sinauer Associates, Sunderland, MA 1992).

15: Diba K, Lester HA, & Koch C. Intrinsic Noise in Cultured Hippocampal Neurons: Experiment and Modeling. *Journal of Neuroscience* **24**, 9723-9733 (2004).

16: Sigg D, Stefani E, & Bezanilla F. Gating current noise produced by elementary transitions in shaker potassium channels. *Science* **264**, 578-582 (1994).

17: Bezanilla F. The voltage sensor in voltage-dependent ion channels. *Physiological Reviews* **80**, 555-592 (2000).

18: Pare D, Shink E, Gaudreau H, Destexhe A, & Lang EJ. Impact of spontaneous synaptic activity on the resting properties of cat neocortical pyramidal neurons in vivo. *J Neurophysiol* **79**, 1450-1460 (1992).

19: Stacey WC, & Durand DM. Synaptic noise improves detection of subthreshold signals in hippocampal CA1 neurons. *Journal of Neurophysiology* **86**:3, 1104-1112 (2001).

20: Jacobson GA, Diba K, Yaron-Jakoubovitch A, Oz Y, Koch C, Segev I, & Yarom Y. Subthreshold voltage noise of rat neocortical pyramidal neurones. *J Physiol* **564**:1, 145-160 (2005).

21: Suffczynski P, Wendling F, Bellanger JJ, & Da Silva JHL. Some insights into computational models of (patho)physiological brain activity. *IEEE Proceedings* **94**:4, 784-804 (2006).

22: Traub RD, Jeffreys JGR, Miles R, Whittington MA, & Toth Katalin. A branching dendritic model of a rodent CA3 pyramidal neurone. *J. Physiol.* **481**:1, 79-95 (1994).

23: Bower JM, & Beeman D. *The Book of GENESIS: Exploring Realistic Neural Models with the Genesis Neural Simulation System, 2nd ed* (TELOS, Santa Clara, Calif. 1998).

24: Traub RD, & Miles R. Pyramidal cell-to-inhibitory cell spike transduction explicable by active dendritic conductances in inhibitory cell. *Journal of Computational Neuroscience* **2**:4, 291-298 (1995).

25: Traub RD, Whittington MA, Colling SB, Buzsaki G, & Jeffreys JGR. Analysis of gamma rhythms in the rat hippocampus in vitro and in vivo. *J. Physiol.* **493**:2, 471-484 (1996).

26: Traub RD, & Miles R. *Neuronal Networks of the Hippocampus* (Cambridge University

Press, New York 1991).

27: Destexhe A, Mainen Zf, & Sejinowski TJ. "Biophysical models of synaptic transmission," in *Methods in Neuronal Modeling* Eds. Koch C, & Seev I, 2nd ed, (MIT Press, Cambridge, MA 1998).

28: Pare D, Lebel E, & Lang EJ. Differential impact of miniature synaptic potentials on the soma and dendrites of pyramidal neurons in vivo. *J Neurophysiol* **78**, 1735-1795 (1997).

29: Menne KML, Folkers A. Malina T, Maex R, & Hofman UG. Test of spike-sorting algorithms on the basis of simulated network data. *Neurocomputing* **44**:46, 1119-1126 (2002).

30: Franks KM, Stevens CF, & Sejnowski TJ. Independent sources of quantal variability at single glutamageric synapses. *Journal of Neuroscience* **23**:8, 3186-3195 (2003).

31: Destexhe A, Mainen ZF, & Sejnowski TJ. Synthesis of models for excitable membranes, synaptic transmission and neuromodulation using a common kinetic formalism. *Journal of Computational Neuroscience* **1**, 195-230 (1994).

32: Mainen ZF, & Sejnowski TJ. "Modeling Active Dendritic Processes in Pyramidal Neurons," in *Methods in Neural Modeling* Eds. Koch C, & Segev I, 2nd ed, (MIT Press, Cambrige, MA 1998).

33: Mott DD, & Lewis DV. The pharmacology and function of central GABAB receptors. *Int Rev Neurobiol.* **36**, 97-223 (1994).

34: Grassberger P, & Procaccia I. Measuring the strangeness of strange attractors. *Physica D: Nonlinear Phenomena* **9**, 189-208 (1983).

35: Takens F. Detectin strange attractors in turbulance. *Brain Topography* **11**, 201-209 (1999).

36: Zalay OC, Kang EE, Cotic M, Carlen PL, & Bardakjian BL. A wavelet packet-based algorithm for the extraction of neural rhythms. *Annals of Biomedical Engineering* **37**:3, 595-613 (2009).

37: Destexhe A, Rudolph M, Fellous JM, & Sejnowski TJ. Fluctuating synaptic conductances recreate in vivo-like activity in neocortical neurons. *Neuroscience* **107**:1, 13-24 (2001).

38: Mody I. Distinguishing between GABAA receptors responsible for tonic and phasic conductances. *Neurochemical Research* **26**:8/9, 907-913 (2001).

39: Mennerick S, Cormier RJ, & Zourumski CF. "Studies of glial glutamate transporters in hippocampal microcultures," in *Transmembrane Transporters* Eds. Quick MW, 1st ed, (John Wiley and Sons, NY, NY 2002).